Solar Physics
DOI: 10.1007/●●●●●-●●●-●●●-●●●●-●

Narrowband spikes observed during the 13 June 2012 flare in the 800-2000 MHz range

Marian Karlický[1] · Ján Rybák[2] · Jan Benáček[3] · Jana Kašparová[1]

Abstract Narrowband (∼5 MHz) and short-lived (∼0.01 s) spikes with three different distributions on the 800-2000 MHz radio spectrum of the 13 June 2012 flare are detected and analyzed. We designate them as SB (spikes distributed in broad band or bands), SZ (spikes distributed in zebra-like bands) and SBN (spikes distributed in broad and narrow bands). Analyzing AIA/SDO images of the active region NOAA 11504, a rough correspondence between groups of the spikes observed on 1000 MHz and peaks in the time profiles of AIA channels taken from the flare sub-area close to the leading sunspot is found. Among types of spikes the SZ type is the most interesting because it resembles to zebras. Therefore, using auto-correlation and cross-correlation methods we compare SZ and SBN spikes with the typical zebra observed in the same frequency range. While the ratio of SZ band frequencies with their frequency separation (220 MHz) is about 4, 5 and 6, in the zebra the frequency stripe separation is about 24 MHz and the ratio is around 50. Moreover, the bandwidth of SZ bands, which consists of clouds of narrowband spikes, is much broader than that of zebra stripes. This comparison indicates that SZ spikes are generated different way than the zebra, but similar way as SBN spikes. We successfully fit the SZ band frequencies by the Bernstein modes. Based on this fitting we interpret SZ and SBN spikes as those generated in the model with Bernstein modes. Thus, the magnetic field and plasma density in the SZ spike source is estimated as about 79 G and 8.4×10^9 cm^{-3}, respectively.

Keywords: Flares, Dynamics; Radio Bursts, Dynamic Spectrum

✉ J. Rybák
rybak@astro.sk

[1] Astronomical Institute, Czech Academy of Sciences, 251 65 Ondřejov, Czech Republic

[2] Astronomical Institute, Slovak Academy of Sciences, Tatranská Lomnica, Slovakia

[3] Center for Astronomy and Astrophysics, Technical University of Berlin, 10623 Berlin, Germany

1. Introduction

Solar radio spikes are observed from tens of MHz up to GHz ranges (Droege, 1977; Karlický, 1984; Staehli and Magun, 1986; Bouratzis et al., 2016; Melnik et al., 2014; Clarkson et al., 2021). They are characterized by short duration (10 - 1000 ms) which decreases with increasing frequency, narrow bandwidth (Δ f/f = 0.002 - 0.01) and the brightness temperature up to 10^{15} K (Benz, 1986; Messmer and Benz, 2000). While Messmer and Benz (2000) studied the spike parameters at two frequency ranges (320-383 MHz and 873-1000 MHz), Nita et al. (2014) presented results for the 1000-1500 MHz range that is the sub-range of the present study (800-2000 MHz). Using the statistical methods they found the minimal and maximal spike bandwidth as (according to their Figure 11): $(\Delta f)_{\rm min} \sim 1$ MHz and $(\Delta f)_{\rm max} \sim 100$ MHz for 1000 MHz and $(\Delta f)_{\rm min} \sim 1$ MHz and $(\Delta f)_{\rm max} \sim 10$ MHz for 1500 MHz. The spikes are of high interest because their understanding can provide detailed information about plasma processes in solar flares on kinetic scales.

Among them, the decimetric-spikes belong to the most interesting because in some cases they are recorded close to the starting frequency of type III bursts and in relation to hard X-ray emissions (Dabrowski and Benz, 2009). As concerns to their spatial localization, such observations are relatively rare. For example, at 327 MHz and 410.5 MHz frequencies of the Nancay Radio Heliograph (Kerdraon and Delouis, 1997), clusters of spikes were observed above the soft and hard X-ray flare sources (Khan and Aurass, 2006). Furthermore, based on spikes observed in the 1 - 1.6 GHz range by Karl G. Jansky Very Large Array (VLA), Luo et al. (2021) proposed that spikes are generated at the termination shock formed above the flare arcade, where a diffuse supra-arcade fan and multitudes of plasma downflows are present. This interpretation is close to the idea that the narrowband dm-spikes are generated by superthermal electrons in the magnetohydrodynamic turbulence in the magnetic reconnection outflows (Karlický, Sobotka, and Jiřička, 1996; Bárta and Karlický, 2001).

On lower frequencies, the LOw Frequency ARray (LOFAR) recorded spikes in the 30 - 70 MHz range that were similar to individual Type IIIb striae observed in the same event (Clarkson et al., 2021). Authors estimated the spike emission region of the order of $\sim 10^8$ cm and brightness temperature as high as 10^{13} K. For these spikes they suggested fundamental plasma emission generated likely by weak/slow electron beams.

Several models of the spikes were suggested. In some of them, the runaway electrons, accelerated in a direct-current electric field, were proposed (Kuijpers, van der Post, and Slottje, 1981; Tajima et al., 1990; Wentzel, 1991). The electron-cyclotron maser (ECM) mechanism, that directly generates electromagnetic waves (spikes), was suggested by Melrose and Dulk (1982), Fleishman and Mel'nikov (1998), Ni et al. (2020) and Melrose (2017). Moreover, Stepanov et al. (1999) and Bárta and Karlický (2001) presented the model, where spike frequencies correspond to those of the upper-hybrid waves, and Willes and Robinson (1996) the model with spike frequencies corresponding to the Bernstein modes.

There is an important additional aspect of the narrowband dm-spikes that is not frequently considered in theoretical models. Namely, seeing them on radio

spectra, dm-spikes are in many cases clustered in bands (clouds) of spikes as was for the first time shown by Krucker and Benz (1994). The authors also found that the frequencies of neighboring bands are in the non-integer ratio (1.06 - 1.54). In the paper by Karlický, Benáček, and Rybák (2021) this result was not only confirmed, but very narrow bands of spikes in the 7 November 2013 event enable to successfully fit the band frequencies by the Bernstein modes.

In the model with the Bernstein modes the loss-cone distribution of superthermal electrons together with much denser Maxwellian background plasma is assumed. In this case, dispersion relations for the Bernstein modes can be written as (Zhelezniakov and Zlotnik, 1975; Karlický, Benáček, and Rybák, 2021)

$$\epsilon_{\parallel}^{(0)} = 1 - 2\omega_{\rm pe}^2 \frac{e^{-\lambda}}{\lambda} \sum_{l=1}^{\infty} \frac{l^2 I_l(\lambda)}{\omega^2 - l^2 \omega_{\rm ce}^2} = 0, \tag{1}$$

$$\omega_{\rm pe}^2 = \frac{n_{\rm e} e^2}{m_{\rm e} \epsilon_0}, \qquad \lambda = \frac{k_\perp^2 v_{\rm tb}^2}{\omega_{\rm ce}^2}, \tag{2}$$

where $\epsilon_\parallel$ is the parallel component of the permittivity tensor, ϵ_0 is the permittivity of free space, $\omega_{\rm pe}$ is the electron plasma frequency, $n_{\rm e}$ is the plasma density of the Maxwellian background plasma, $\omega_{\rm ce}$ is the the electron cyclotron frequency, $\mathbf{k} = (k_\parallel, k_\perp)$ is the wave vector parallel and perpendicular to the direction of the magnetic field, respectively, ω is the wave frequency of the electrostatic wave, $I_l(\lambda)$ is the modified Bessel function of lth order, λ is the dimensionless parameter, $m_{\rm e}$ is the electron mass, and e is the electron charge.

While the Maxwellian background plasma determines the dispersion relation of the Bernstein modes, a generation of these electrostatic waves is owing to the instability caused by electrons with the loss-cone distribution. The Bernstein modes can be unstable if the double plasma resonance condition is fulfilled

$$\omega - \frac{k_\parallel u_\parallel}{\gamma_{\rm rel}} - \frac{s\omega_{\rm ce}}{\gamma_{\rm rel}} = 0, \tag{3}$$

where $\gamma_{\rm rel} = (1 - v^2/c^2)^{-\frac{1}{2}}$ is the relativistic Lorentz factor and s is the resonance gyro-harmonic number. Their growth rate for some specific $(\omega, k_\perp)$ can be calculated as (Zhelezniakov and Zlotnik, 1975)

$$\gamma(\omega, k_\perp) = -\frac{{\rm Im}\, \epsilon_\parallel^{(1)}}{\left[\frac{\partial {\rm Re}\, \epsilon_\parallel^{(0)}}{\partial \omega}\right]_{\epsilon_\parallel^{(0)}=0}}. \tag{4}$$

We note that entirely the same equations are used for generation of the upper-hybrid waves in the double-plasma resonance (DPR) model of solar radio zebras (Zlotnik, 2013). In both these models it is assumed that the Bernstein or upper-hybrid (electrostatic waves) are converted to the observed electromagnetic waves by coalescence processes with the low-frequency waves or mutual coalescence of the Bernstein modes. But, there is an essential difference in these models. While in the model with the Bernstein modes the Bernstein modes and escaping

electromagnetic waves are produced in one source, in the case of the zebra model with the upper-hybrid wave the zebra-stripes are generated at different locations.

In this paper, after short statistics of spikes observed in the 800-2000 MHz range by the Ondřejov radiospectrograph (Jiřička and Karlický, 2008), we present the narrowband spikes, observed during the 13 June 2012 flare. We study these spikes because three different types of spikes distributions were detected on the radio spectrum of a single flare: a) spikes distributed in broad band or bands, b) spikes distributed in zebra-like bands, and c) spikes distributed in broad and narrow bands. We also search for their counterparts in intensity variations in localized places of a flare in AIA/SDO images. We compare the spikes in zebra-like bands with a typical zebra in the same frequency range in order to distinguish their generation mechanisms. Finally, we discuss the model of the presented spikes.

2. Observations

In Table 1 we present 18 spike events (consisting sometimes several groups of spikes) observed in years 2007-2020 by the 800-2000 MHz Ondřejov radiospectrograph with the time and frequency resolution of 0.01 s and 4.7 MHz, respectively (Jiřička and Karlický, 2008). As can be seen here, these events are always associated with flares (1 flare classified as B flare, 8 classified as C flare, and 9 classified as M flare). Most of the events were recorded before the GOES (Geostationary Operational Environmental Satellites) soft X-ray flare maximum (12 BM, see Table 1), one before and during the maximum (1 BM, M), one before and after the maximum (1 BM, AM), one before and after the maximum, but during bump on the GOES X-ray profile (1 BM, BAM), one after the maximum, but during bump on the GOES X-ray profile (1 BAM), and two events during the pre-flare phase (2 PF). As shown in Table 1, most of these spike events were associated with the hard X-ray (HXR) emission observed by RHESSI or Fermi GBM instruments (Lin et al., 2002; Meegan et al., 2009). All these facts indicate that spikes are generated during the impulsive phases of solar flares.

2.1. The 13 June 2012 spike event

Among these spike events the most interesting examples of spikes were observed during the 13 June 2012 flare. During this flare we registered many groups of spikes and also their different types. According to the GOES X-ray observation this M1.2 flare started at 11:29 UT, maximum at 13:17 UT and ended at 14:31 UT. In H_α observation it started at 11:36 UT, maximum at 14:41 and ended at 16:23 UT; lasting thus about 5 hours. It occurred at the position S16E18 in the active region NOAA AR 11504 with an importance 1N.

In this flare in the time interval 13:00-13:30 UT we observed eleven groups of spikes, see Figure 1. This time interval covers only a part of this long flare around its GOES X-ray maximum. Detailed radio spectra of three groups of spikes (group 1, 3 and 9 in Table 2) are shown in Figure 2. As can be seen here, spikes at these groups differ. Therefore, we classified them according to

Table 1. Spike events and corresponding hard X-ray (HXR) emission and GOES flares. HXR energy range corresponds to the highest range detected during the radio spike time interval. RHESSI data were the primary source for the HXR emission. If RHESSI data were not available, Fermi GBM data were used, see mark f. For the 04-Sep-14 event, RHESSI HXR data, denoted by *, are available several seconds after the spike event, from 13:19 UT. Abbreviations in Notes mean: BM spikes before the GOES maximum, M spikes at the maximum, AM spikes after the maximum, BAM spikes during the bump on the GOES flare decay profile, and PF spikes in the preflare phase.

Spike Event		Flares (HXR, GOES)				
Time interval (UT)	Range (GHz)	HXR (keV)	Start (UT)	Max (UT)	Class	Notes
12–Feb–10 09:40:40–09:41:20	0.8–1.1	25–50	09:38	09:42	B9.6	BM
16–Feb–11 14:23:00–14:25:40	0.8–2.0	50–100	14:19	14:25	M1.6	BM,M
18–Feb–11 10:13:30–10:14:30	0.8–2.0	50–100	09:55	10:11	M6.6	AM
04–Mar–12 10:37:40–10:41:10	0.8–1.6	50–100[f]	10:29	10:52	M2.0	BM
13–Jun–12 13:02:40–13:30:00	0.8–1.8	50–100	11:29	13:17	M1.2	BM,AM
14–Jun–12 10:39:30–10:42:30	0.8–2.0	12–25	10:45	10:50	C2.5	PF
14–Jun–12 11:00:10–11:00:50	0.8–2.0	no data	11:05	11:12	C5.0	PF
11–Apr–13 06:56:00–07:02:00	0.8–2.0	50–100	06:55	07:16	M6.5	BM
07–Nov–13 12:26:00–12:28:30	0.8–2.0	no data	12:22	12:29	C5.9	BM
08–May–14 10:02:10–10:04:00	0.8–2.0	100–300[f]	09:59	10:07	M5.2	BM
09–Jun–14 12:27:10–12:37:00	0.8–2.0	50–100	12:24	12:29	C9.0	BM,BAM
11–Jun–14 05:41:10–05:42:00	0.8–1.6	12–25	05:30	05:34	M1.8	BAM
11–Jun–14 07:11:40–07:12:00	0.8–2.0	25–50	07:09	07:12	C2.8	BM
12–Jun–14 09:33:50–09:36:50	0.8–1.3	100–300[f]	09:23	09:37	M1.8	BM
12–Jun–14 15:59:30–15:59:50	0.8–1.6	25–50	15:57	16:03	C7.8	BM
04–Sep–14 13:17:50–13:18:50	1.1–1.8	12–25[*]	13:10	13:30	C6.3	BM
12–Sep–14 09:31:20–09:32:00	1.0–1.4	14–25[f]	08:24	09:55	C3.2	BM
22–Aug–15 06:41:40–06:42:50	0.8–1.6	no data	06:39	06:49	M1.2	BM

their appearance in the radio spectrum as SB (spikes distributed in broad band or bands) (Figure 2a), SZ (spikes distributed in zebra-like bands) (Figure 2b), and SBN (spikes distributed in broad and narrow bands) (Figure 2c). Owing to resemblance of SZ and zebras, in the following we will make a comparison of SZ spikes with a typical zebra observed in the same frequency range (Figure 6). We will also compare SZ spikes with SBN spikes.

Using this classification we classified all groups of spikes in the 13 June 2012 flare, see Table 2. In this table also the basic parameters of these spike groups are summarized: type, maximal number of the frequency bands of spikes (MNFB) and characteristic ratios of neighboring bands of spikes (BR). These ratios were computed from the frequencies at flux maxima of spike bands. On lower frequencies in the 200-400 MHz range at 13:08-13:24 UT these spike groups were associated with Type II burst (Callisto-BLEN7M observation).

AIA/SDO UV (Lemen et al., 2012), HMI/SDO (Scherrer et al., 2012; Schou et al., 2012) and RHESSI X-ray (Lin et al., 2002) observations associated with these groups of spikes are shown in Figure 3 and 4. As seen in Figure 4 (middle

Table 2. Basic parameters of groups of spikes observed during the 2012 June 13 flare: times, frequency range, types, maximal number of the frequency bands of spikes (MNFB) and characteristic ratios of neighboring bands of spikes (BR). SB denotes spikes in broadbands, SZ means spikes in zebra-like bands, and SBN means spikes in broad and narrow bands.

No	Time (UT)	Range (GHz)	Type	MNFB	BR
1	13:02:42-13:02:58	0.8-1.3	SB	1	-
2	13:11:48-13:12:40	0.8-1.2	SZ	2	1.21
3	13:13:06-13:14:06	0.8-1.8	SZ	4	1.16, 1.19, 1.21
4	13:14:38-13:14:50	0.8-1.6	SZ	4	1.15, 1.18, 1.23
5	13:16:55-13:17:25	0.8-1.5	SB	1	-
6	13:21:08-13:21:26	0.8-1.6	SB	1	-
7	13:22:21-13:23:18	0.8-1.8	SB	1	-
8	13:24:25-13:24:57	0.8-1.8	SBN	3	1.25, 1.26
9	13:26:12-13:26:36	0.8-1.8	SBN	3	1.22, 1.24
10	13:26:59-13:27:30	1.0-1.6	SZ	2	1.08
11	13:28:55-13:29:05	0.8-1.6	SB	1	-

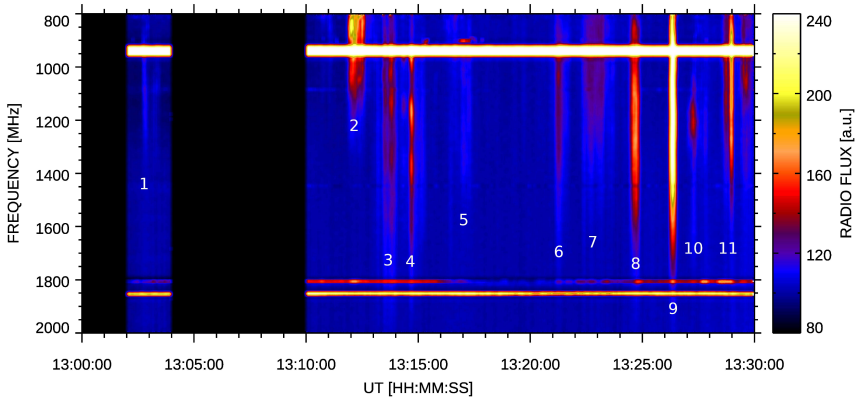

Figure 1. The 800-2000 MHz overview radio spectrum observed at 13:10:00 - 13:30:00 UT during the 13 June 2012 flare by the Ondřejov radiospectrograph. Black parts of radio spectrum at 13:00:00-13:02:00 and 13:04:00-13:10:00 UT mean that we have no data in these intervals because they were not archived owing to no bursts there.

part), in the time interval of spikes groups, the RHESSI X-rays exhibit a slow decrease in time with some enhancements; see e.g. that just before the GOES flare maximum. They indicate a presence of superthermal electrons with the energy up to 100 keV at these times. Owing to RHESSI technical problems, X-ray source positions could not be constructed. Therefore, using AIA/SDO observations we tried to localize a part of the flare where temporal intensity variations correspond to variations at the 1000 MHz time profile (Figure 4). Searching the time profiles in AIA channels (1700, 304, 171, 335 and 94 Å and continuum) in small regions (starting from those with 20 × 20 arcsec) in the

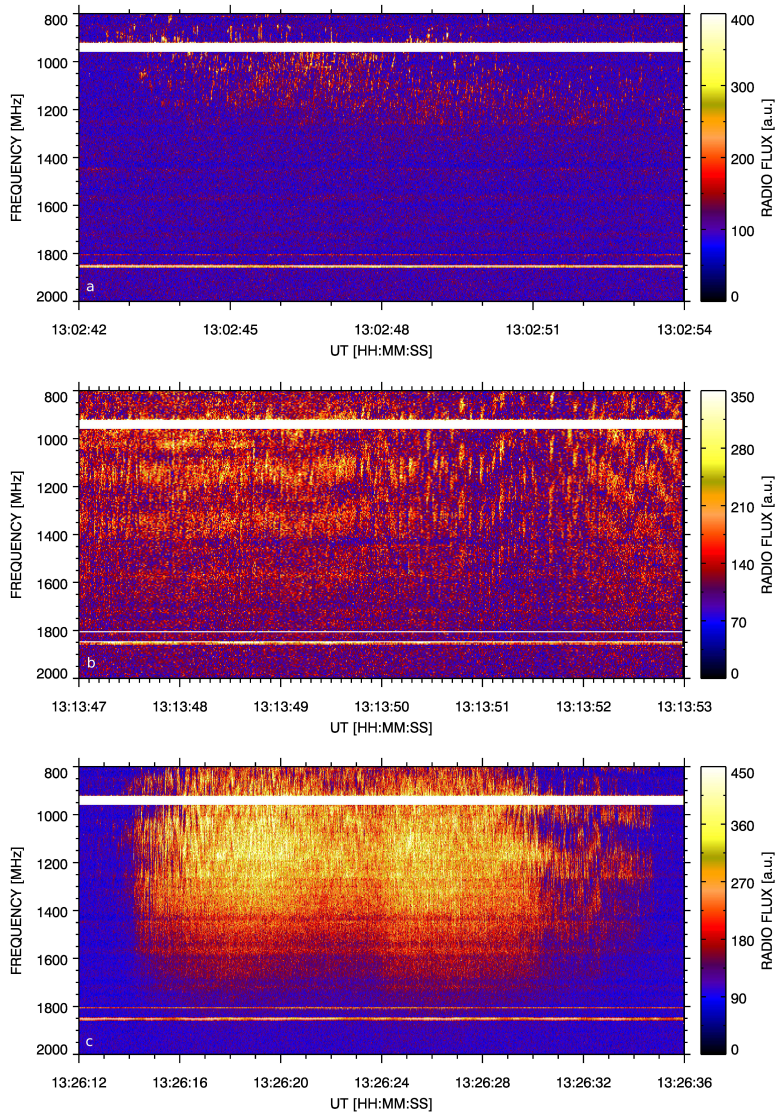

Figure 2. Examples of spikes observed during the 13 June 2012 flare: a) The radio spectrum observed at 13:02:42 - 13:02:54 UT showing spikes classified as SB (group 1, see Table 2 and Figure 1). b) The radio spectrum observed at 13:13:47 - 13:13:53 UT showing spikes classified as SZ (part of group 3). c) The radio spectrum observed at 13:26:12 - 13:26:36 UT showing spikes classified as SBN (group 9).

whole flare site we found the most interesting correspondence with the 1000 MHz radio profile in the white rectangle with the coordinates X=-270– -235 and Y=-298 – -280 arcsec (Figure 3 and 4). It is interesting that this position corresponds to one end of the sigmoidal flare structure where many magnetic field lines of flare loops are concentrated; rooted in the area of the northern part of the active region leading sunspot, see HMI continuum and magnetogram in Figure 3. In other positions AIA profiles were smoother and without such distinct variations, or with some variations, but only in one AIA channel. As seen in Figure 4, there are peaks in several AIA channels observed simultaneously that correspond to peaks in the 1000 MHz profile. While peaks in 94 Å indicate a presence of a hot plasma (6.3×10^6 K), the 1700 Å peaks show a heating of deep atmospheric layers with the temperature 5.0×10^3 K, probably owing to precipitating superthermal particles. The peaks in radio and AIA are of varying sizes, not all peaks on the 1000 MHz radio profile have corresponding peaks in AIA channels. It indicates a complex relation. In fact, a simple relation cannot be expected because it is commonly assumed that spikes are generated by superthermal electrons with the loss-cone distribution, but peaks in the AIA channels express plasma density enhancements at the AIA channel characteristic temperature.

3. Analysis of spikes, comparison with typical zebra in the same frequency range and modelling of SZ frequencies

Radio observations show three types of spikes distributions: a) in one cloud of spikes (SB), b) in several zebra-like bands (SZ), and c) clouds of spikes with very narrow bands of spikes (SBN). The presented SBN type of spikes is similar to the event from 7 November 2013 that was interpreted as the emission on Bernstein modes (Karlický, Benáček, and Rybák, 2021). To confirm this similarity we computed cross-correlation at three spike-band frequencies from the ending part of SBN: 990, 1220, and 1490 MHz (Figure 5), where the spike bands are the narrowest. We found that the time lag is ≤ 0.01 s, in agreement with the 7 November 2013 case. The maximal cross-correlation in Figure 5 is even higher than that in Figure 3 in the paper by Karlický, Benáček, and Rybák (2021). Thus, we think that the present SBN spikes are of the same origin as the spikes observed at 7 November 2013, i.e., the emission is generated on Bernstein modes. Furthermore, we compare SB and broad part of SBN spikes. Owing to the similar parameters of individual spikes we think that the SB type is as one broad part of SBN type.

3.1. Comparison of zebra-like spikes (SZ) with the zebra in the same frequency range

The most interesting type of spikes is the SZ type because it resembles zebras. Therefore, let us compare it with the typical zebra in the same frequency range, e.g., with the zebra observed at 1 August 2010 (Figure 6 upper part). First, we use the auto-correlation method. We computed a time evolution of the auto-correlations along frequencies. We made these computations for SZ shown in

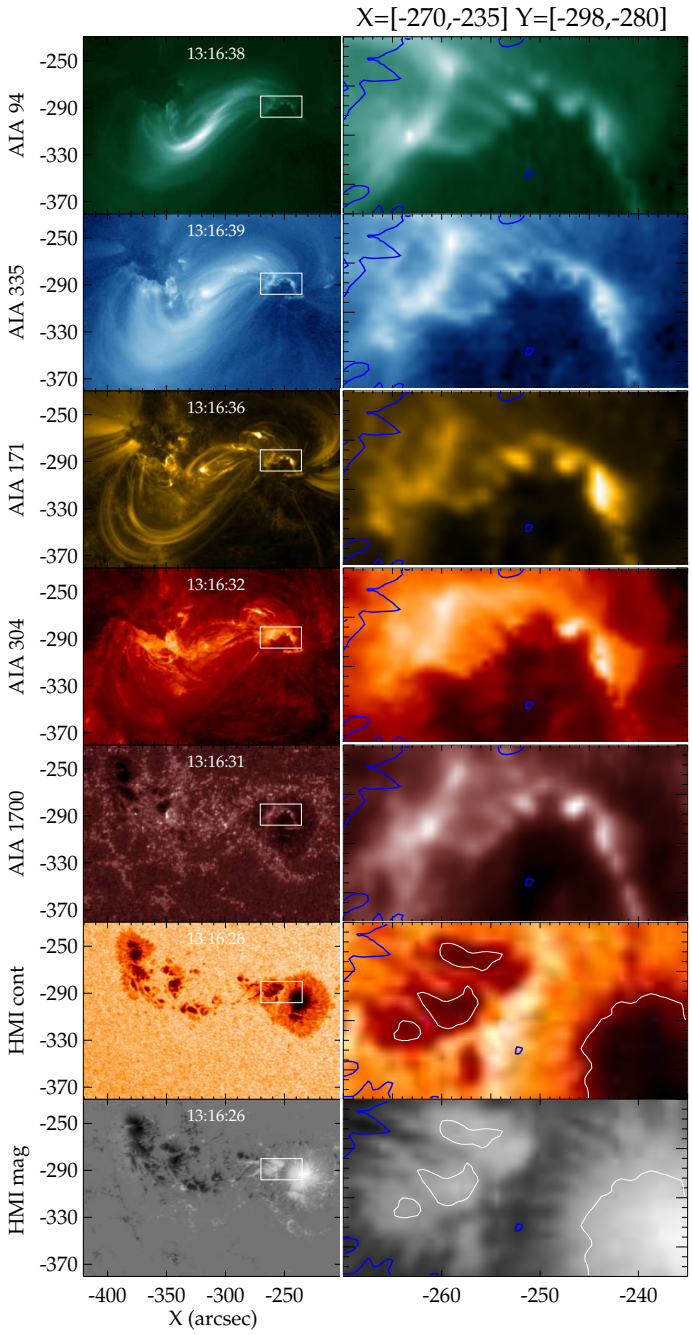

Figure 3. The AIA/SDO and HMI/SDO images of the flare overall region (left) and zoom region (right), delineated by the white rectangle in the overall images, for five AIA channels (94, 335, 171, 304, 1700 Å) and the HMI continuum and magnetogram at the time close to the flare maximum (13:16:36 UT). White isolines in the HMI continuum and magnetogram zoom region images stem for contours of the leading sunspot umbra and three nearby pores. Blue isolines denote the neutral division lines between the northern and southern magnetic polarities.

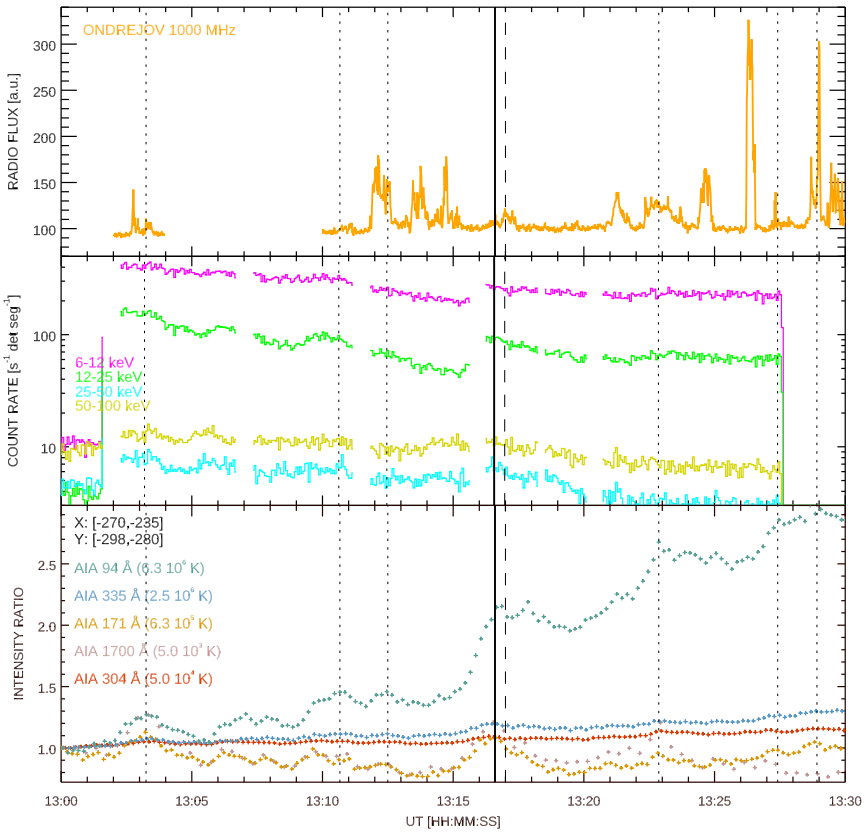

Figure 4. Time profiles in the interval of the radio spectrum (Figure 1, at 13:00 - 13:30 UT) of the flux on 1000 MHz (upper part) and RHESSI counts (middle part) together with AIA light curves (bottom part, expressed as the ratio to the AIA intensity at times around 13 UT) taken from the small white rectangle in Figure 3. The vertical full, dashed and dotted lines in plots of time profiles mean the time of AIA images in Figure 3, the GOES flare maximum, and times of some peaks in the 94 Å time profile, respectively.

Figure 2b and also for the ending part of SBN in Figure 2c and the zebra shown in Figure 6 upper part. The results are in Figure 7. The auto-correlations of type SZ and SBN are similar. Their frequency lag is about 220 and 250 MHz, respectively, and this lag is practically constant in time. When we divide the mean SZ band frequencies (∼960, ∼1120, ∼1330 and ∼1550 MHz) by the lag frequency (∼220 MHz) the ratios ∼4.4, ∼5.1, ∼6.0 and ∼7.0 can be obtained. Similarly, dividing the mean SBN band frequencies at the ending part of SBN (∼990, ∼1220 and ∼1490 MHz) by the lag frequency (∼250 MHz) the ratios ∼4.0, ∼4.9 and ∼6.0 are obtained. On the other hand, the auto-correlations of the zebra differ essentially. The frequency lag at first harmonic is about 24 MHz.

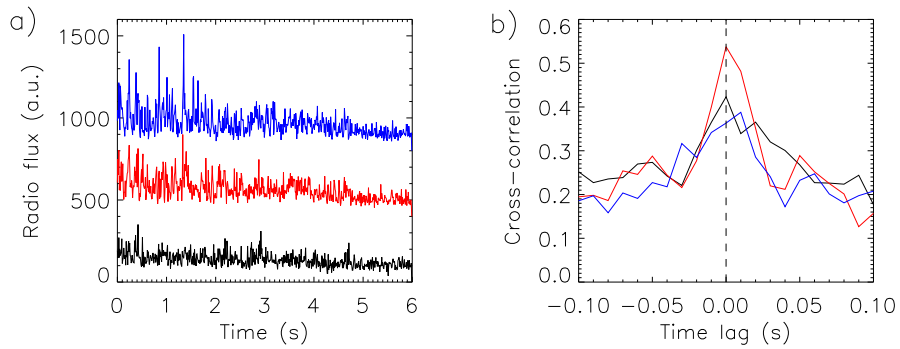

Figure 5. Case with SBN: a) Radio flux in dependence on time at 1490 MHz (black line), at 1220 MHz (red line) + 400 a.u., and at 990 MHz (blue line) + 800 a.u., starting at 13:26:30 UT in the 13 June 2012 event and lasting 6 s. b) Cross-correlations of the radio flux profiles on 1490 and 1220 MHz (black line), 1220 and 990 MHz (red line), and 1490 and 990 MHz (blue line).

When the mean zebra frequency ($\sim$ 1250 MHz) is divided by the lag frequency ($\sim$ 24 MHz) then this ratio is about 52.

Moreover, the frequency lag in the zebra case is varying in time as seen on higher harmonics of time lags. To understand better what it means, we calculated the frequency intervals between neighboring zebra stripes at three time instants (Figure 6 bottom part). As shown here, for the zebra stripes numbered 1 and 2 the frequency interval between them (see the short horizontal lines) changes from 23.5 MHz to 23.5 MHz and to 28.2 MHz, and for the zebra stripes numbered 4 and 5 the frequency interval between them changes from 14.1 MHz to 18.8 MHz and to 28.2 MHz. (Note that the frequency resolution of the radio spectrum is 4.7 MHz.) It means that the frequency interval between the neighboring zebra stripes changes and this frequency interval can be different from those between other zebra stripes. This irregular variation of the separation frequency indicates that zebra-stripe sources cannon be generated on the Bernstein modes in one source region. In the double-plasma resonance models of zebras this variation is interpreted by waves propagating along the loop where the zebra-stripe sources are located (Karlický and Yasnov, 2021). We also found that the bandwidth of SZ bands is much broader than that of zebra stripes. While in the SZ case it is about 200 MHz in the zebra case it is about 10 MHz.

3.2. Modelling of SZ frequencies by Bernstein modes

To confirm a similarity between SZ and SBN of the 13 June 2012 flare given by auto-correlations (Figure 7) and SBN observed in 7 November 2013 with the Bernstein modes, we fitted the mean SZ band frequencies by the same way as in the SBN 7 November 2013 case (Karlický, Benáček, and Rybák, 2021), see also Benáček and Karlický (2019). Firstly, we searched for the time where the bandwidth of SZ spike bands is the narrowest. We found it for 13:13:50.8 UT where we determined the mean spike band frequencies as 860, 1070, 1290 and 1510 MHz

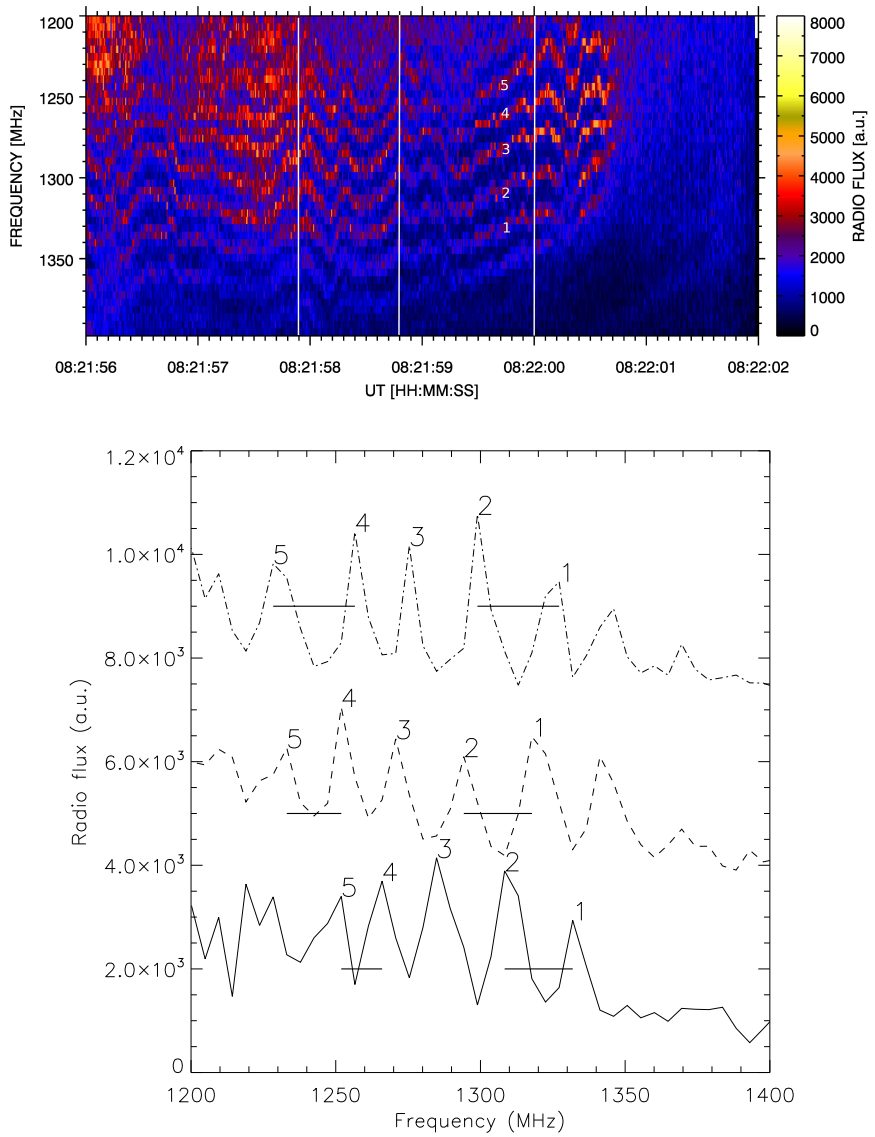

Figure 6. Upper: The 1200-1400 MHz radio spectrum showing the zebra observed during the 1 August 2010 flare. The white vertical lines and numbers 1-5 show the times of the frequency profiles and selected zebra stripes shown in bottom part of the Figure. Bottom: Radio flux vs. frequency profiles: the full line means the radio flux at 08:21:57.9 UT, dashed line means the radio flux + 3500 a.u. at 08:21:58.8 UT, and dashed-dotted line means the radio flux + 7000 a.u. at 08:22:00.0 UT. Numbers 1-5 designate zebra stripes; see the upper part. Short horizontal lines show the frequency intervals between zebra stripes 1 and 2 and zebra stripes 4 and 5 at three instants 08:21:57.9, 08:21:58.8 and 08:22:00.0 UT.

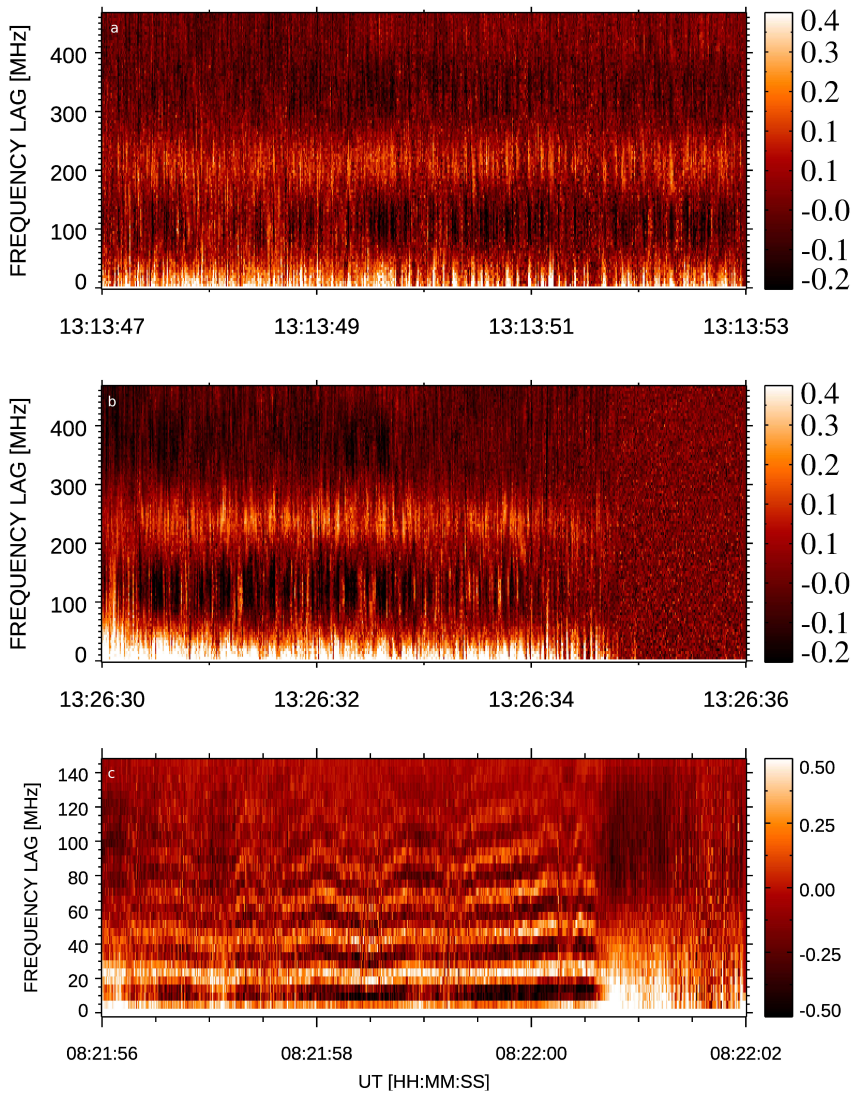

Figure 7. Auto-correlation of the radio fluxes vs. radio spectrum frequency. a) SZ case in the time interval 13:13:47-13:13:53 UT. b) SBN case in the time interval 13:26:30-13:26:36 UT. c) Zebra case in the 1200-1400 MHz range observed at 08:21:56-08:22:02 UT in August 1, 2010.

(for $s = 4$ - 7). Then using Equations 1 and 3 we fitted these band frequencies by calculating the dispersion curves of the Bernstein modes and corresponding growth rates and assuming that Bernstein modes correspond to observed radio frequencies. The best fit is shown in Figure 8. This fit was obtained for the following parameters: $n_e/n_h = 15, v_t/c = 0.25, v_{tb}/c = 0.01834$ ($T_b = 2MK$), $\omega_{pe}/\omega_{ce} = 3.85$, and $f_{pe} = 827$ MHz, where $f_{pe} = \omega_{pe}/(2\pi)$, n_e/n_h is the ratio between the electron plasma densities of the background and hot compo-

nent plasma, $v_{\rm t}$ and $v_{\rm tb}$ are the characteristic velocities of hot and Maxwellian background plasmas, T_b is the temperature of the background plasma, and c is the light speed.

Now, considering the frequency separation between spike bands as follow from the above analysis (220 MHz) and the plasma frequency as $f_{\rm pe} = 827$ MHz, the magnetic field and plasma density in the spike source can be estimated as about 79 G and 8.4×10^9 cm^{-3}, respectively.

A question also arises what is the expected bandwidth of spikes in the model with Bernstein modes. But, it is a very complex problem. Therefore, let us estimate only the Bernstein mode bandwidth for several gyro-harmonic numbers s, assuming that this bandwidth is formed only by density variations. We take these variations as $\Delta n/n \approx 1/\sqrt{n} \approx 1.1 \times 10^{-5}$ (statistical noise). Then, the frequency variation at the present plasma frequency (827 MHz) is about 2.7 MHz. We estimated the linearized bandwidths in region of each branch, where its growth rate is maximal. We found the bandwidth of Bernstein modes with $s = 4, \ldots, 7$ as 0.9, $3\times\ 10^{-3}$, $5\times\ 10^{-5}$ and $5\times\ 10^{-5}$ MHz, respectively. The bandwidths narrow as the permittivity derivation nonlinearly increases with increasing of the gyro-harmonic number. For all s, the Bernstein mode bandwidth is smaller than the minimal spike bandwidth found by Nita et al. (2014) ($\sim$ 1 MHz). However, the problem of the spike bandwidth is much more complex. It is due to not only effects of density and magnetic field variations, but also due to the conversion of Bernstein modes into the electromagnetic waves. Moreover, density and magnetic field variations are probably interconnected.

4. Discussion and conclusions

We confirmed that the narrowband dm-spikes are mostly observed during the impulsive flare phases, see Table 1. As follows from Table 2 and analysis of the 13 June 2012 spike event, dm-spikes are observed in bands with the non-integer ratio in the interval 1.08–1.26; in agreement with the result of Krucker and Benz (1994). We note that this result is not frequently considered in theoretical models of dm-spikes.

In the analysis of the 13 June 2012 spike event we tried to search for some relation between the 1000 MHz time profile (with groups of spikes) and variations of intensities in selected flare places using AIA/SDO observations. The most interesting relation was found for AIA intensities taken from one end of the sigmoidal flare structure where many magnetic field lines of flare loops are concentrated (Figure 3 and 4). The peaks in radio and AIA (Figure 4) are of varying sizes, not all peaks on the 1000 MHz radio profile have corresponding peaks in AIA channels. It indicates that their relation is not simple. In reality, a simple relation cannot be expected because spikes are generated by superthermal electrons with the loss-cone distribution while peaks in the AIA channels indicate plasma density enhancements at the AIA channel characteristic temperature.

During one flare from 13 June 2012 we observed spikes with three different types: SB, SZ and SBN spikes. Analyzing SBN spikes in their narrowband part by the cross-correlation method we found that the SBN spikes are similar to

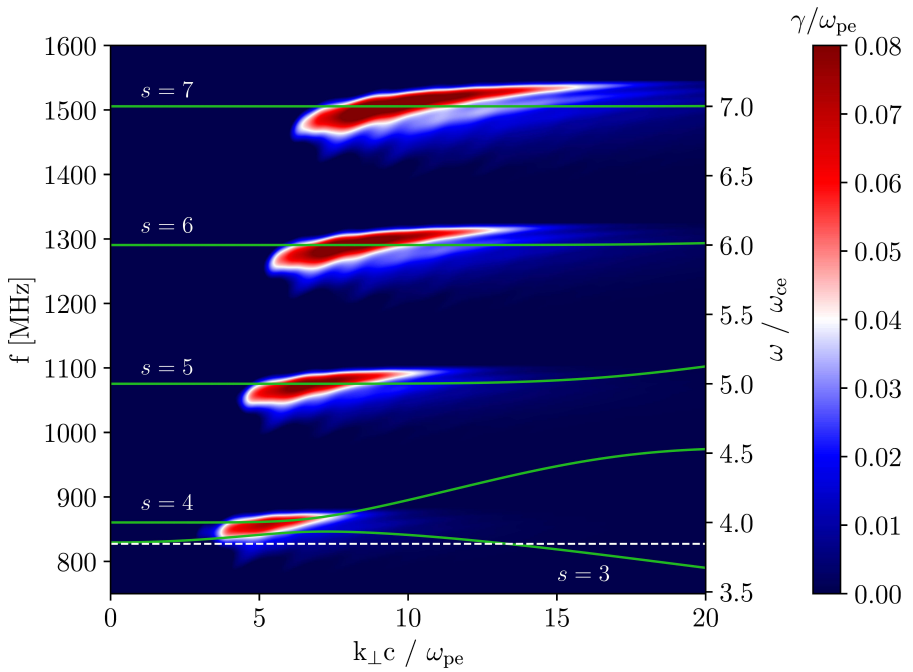

Figure 8. Growth rates of the Bernstein modes as a function of the frequency and perpendicular k-wave vector for parameters $\omega_{pe}/\omega_{ce} = 3.85, v_{tb}/c = 0.01834, v_t/c = 0.25, n_e/n_h = 15$. The values of f in MHz correspond to the radio emission on Bernstein modes, i.e. $\omega_{pe} = 2\pi f_{pe}$, $f_{pe} = 827$ MHz. *Green lines:* Dispersion branches computed from the Equation 1, s is the gyro-harmonic number of each branch. *White dashed horizontal line:* Plasma frequency.

those presented in the paper by Karlický, Benáček, and Rybák (2021). Thus, we interpret SBN similarly, i.e., as generated on Bernstein modes. We also found a similarity in autocorrelations of SZ and SBN ending part which speaks in favor of the same generation mechanism for these spikes.

We made a detailed comparison of the 13 June 2012 SZ (zebra-like) spikes with the typical zebra in the same frequency range that was observed at 1 August 2010. We found the following differences: In the SZ case: The separation frequency Δf between neighboring spike bands is about 220 MHz. The autocorrelation in SZ expresses low variability in time. The ratios between four spike-bands and separation frequencies was found as 4.4, 5.1, 6.0 and 7.0. Similarly, in the SBN case these ratios for three spike bands are 4.0, 4.9 and 6.0. On the other hand, in the zebra case: The separation frequency Δf between neighboring zebra stripes is about 24 MHz. The variability of the autocorrelation in time in the zebra case is higher than in SZ case. Furthermore, the ratio between the mean zebra-stripe frequency and separation frequency is about 1250 MHz/24 MHz $\sim$ 52.

Moreover, we found that the separation frequency between neighboring zebra stripes changes by different way for different pairs of the neighboring zebra stripes (Figure 5). This irregular variation of the separation frequency excludes

that the analyzed zebra is generated in one source as is in the model with the Bernstein modes.

The bandwidth of of SZ spike bands (consisting many narrowband spikes) is much broader than that of zebra stripes. For this reason it was impossible to make the similar analysis of time evolution of band (or spike) separation frequencies as in the zebra case shown in Figure 6 bottom part.

Nevertheless, at time of the narrowest SZ bands we successfully fitted SZ frequencies by the model with the Bernstein modes. Using the parameters in this model we estimated the mean magnetic field strength and plasma density in the SZ source as about 79 G and 8.4×10^9 cm^{-3}, respectively. We propose that broad bands of SZ spikes correspond to a region with some interval of the magnetic field and density. In accordance with our previous ideas (Karlický, Sobotka, and Jiřička, 1996; Bárta and Karlický, 2001) we think that this region is in the magnetic reconnection outflow, where the plasma is in the turbulent state.

Considering all these facts, we conclude that SZ and SBN spikes observed in 13 June 2012 were generated according to the model with the Bernstein modes. We believe that the parameters, e.g. the ratio between the band (stripe) and separation frequencies, found in the analysis of SZ spikes and the 1 August 2010 zebra, can help in interpretations of other observed SZ spikes and zebras.

In Section 3.2 we tried to estimate the spike bandwidth in the model with Bernstein modes. We considered only the Bernstein mode bandwidth assuming only an effect of the density variations. But this problem is much more complex. It is due to not only effects of density and magnetic field variations, but also due to the conversion of Bernstein modes into the electromagnetic waves. Moreover, density and magnetic field variations are probably interconnected. Therefore, the question about the spike bandwidth remains open and further theoretical analysis is necessary.

Similarly as in other solar radio bursts, the radio-wave scattering can play a role also in spikes. The scattering is proportional to $(f_{pe}/f)^2$ (Benz, 1993), where f_{pe} is the plasma frequency and f is the frequency of the radio emission. The scattering depends on the size of the scattering region, sizes and density irregularities. The scattering enhances sizes of the radio sources and causes temporal smoothing of time variations of the burst intensity. Moreover, there is the wave ducting of the radio emission (Duncan, 1979) that requires "fibrous" structures of the plasma density (Kuznetsov et al., 2020). To provide the scattering rate comparable with that of the observations, magnetic tubes would need to have the density contrast of $\Delta n/n \gg 1$ (e.g. Robinson (1983) request a 25-fold increase of the plasma density over dense fibres in the ducting model). Existence of such structures in the solar corona is not supported by EUV observations (e.g. Motorina, Fleishman, and Kontar, 2020). So the "ducting" model is quantitatively inconsistent with the observations and anisotropic scattering is required.

In the present study without spike source imaging, the scattering can only smooth and prolong duration of spikes. But, the parameters of the scattering region are not known. We found that the plasma frequency for the narrowest spike bands at 13:13:50.8 UT is 827 MHz and Bernstein mode frequencies are 860, 1070, 1290, and 1510 MHz. Because the lowest Bernstein frequency 860

MHz is 33 MHz above the plasma frequency that is why the scattering of spike emission in the model with Bernstein modes is less important than the scattering in the case of the radio emission on the fundamental frequency ($f \sim f_{pe}$) as e.g., in the type III bursts. For Bernstein modes with increasing s the effect of scattering decreases.

Acknowledgments M. K. acknowledges support from the project RVO-67985815 and GA ČR grants 20-09922J, 20-07908S, 21-16508J and 22-34841S. J.R. support by the Science Grant Agency project VEGA 2/0048/20 (Slovakia), J.B. support by the German Science Foundation (DFG) project BU 777-17-1, and J. K. support by GA ČR grant 19-09489S. Help of the Bilateral Mobility Project SAV-18-01 of the SAS and CAS is acknowledged as well. We also acknowledge the use of the Fermi Solar Flare Observations facility funded by the Fermi GI program. Data supplied courtesy of the SDO/HMI and SDO/AIA consortia.

References

Bárta, M., Karlický, M.: 2001, Turbulent plasma model of the narrowband dm-spikes. *Astron. Astrophys.* **379**, 1045. DOI. ADS.

Benáček, J., Karlický, M.: 2019, Growth Rates of the Electrostatic Waves in Radio Zebra Models. *Astrophys. J.* **881**, 21. DOI. ADS.

Benz, A.O.: 1986, Millisecond Radio Spikes. *Solar Phys.* **104**, 99. DOI. ADS.

Benz, A.O.: 1993, *Plasma astrophysics: Kinetic processes in solar and stellar coronae* **184**. DOI. ADS.

Bouratzis, C., Hillaris, A., Alissandrakis, C.E., Preka-Papadema, P., Moussas, X., Caroubalos, C., Tsitsipis, P., Kontogeorgos, A.: 2016, High resolution observations with Artemis-IV and the NRH. I. Type IV associated narrow-band bursts. *Astron. Astrophys.* **586**, A29. DOI. ADS.

Clarkson, D.L., Kontar, E.P., Gordovskyy, M., Chrysaphi, N., Vilmer, N.: 2021, First Frequency-time-resolved Imaging Spectroscopy Observations of Solar Radio Spikes. *Astrophys. J. Lett.* **917**, L32. DOI. ADS.

Dabrowski, B.P., Benz, A.O.: 2009, Correlation between decimetric radio emission and hard X-rays in solar flares. *Astron. Astrophys.* **504**, 565. DOI. ADS.

Droege, F.: 1977, Millisecond fine-structures of solar burst radiation in the range 0.2 - 1.4 GHz. *Astron. Astrophys.* **57**, 285. ADS.

Duncan, R.A.: 1979, Wave ducting of solar metre-wave radio emission as an explanation of fundamental/harmonic source coincidence and other anomalies. *Solar Phys.* **63**, 389. DOI. ADS.

Fleishman, G.D., Mel'nikov, V.F.: 1998, REVIEWS OF TOPICAL PROBLEMS: Millisecond solar radio spikes. *Physics Uspekhi* **41**, 1157. DOI. ADS.

Jiřička, K., Karlický, M.: 2008, Narrowband Pulsating Decimeter Structure Observed by the New Ondřejov Solar Radio Spectrograph. *Solar Phys.* **253**, 95. DOI. ADS.

Karlický, M.: 1984, Narrowband DM Spikes as Indication of Flare Mass Ejection. *Solar Phys.* **92**, 329. DOI. ADS.

Karlický, M., Yasnov, L.V.: 2021, Spatial quasi-periodic variations of the plasma density and magnetic field in zebra radio sources. *Astron. Astrophys.* **646**, A179. DOI. ADS.

Karlický, M., Benáček, J., Rybák, J.: 2021, Narrowband Spikes Observed during the 2013 November 7 Flare. *Astrophys. J.* **910**, 108. DOI. ADS.

Karlický, M., Sobotka, M., Jiřička, K.: 1996, Narrowband dm-Spikes in the 2 GHz Frequency Range and MHD Cascading Waves in Reconnection Outflows. *Solar Phys.* **168**, 375. DOI. ADS.

Kerdraon, A., Delouis, J.-M.: 1997, In: Trottet, G. (ed.) *The Nançay Radioheliograph* **483**, 192. DOI. ADS.

Khan, J.I., Aurass, H.: 2006, Observations of the coronal dynamics associated with solar radio spike burst emission. *Astron. Astrophys.* **457**, 319. DOI. ADS.

Krucker, S., Benz, A.O.: 1994, The frequency ratio of bands of microwave spikes during solar flares. *Astron. Astrophys.* **285**, 1038. ADS.

Kuijpers, J., van der Post, P., Slottje, C.: 1981, Runaway acceleration in a radio flare. *Astron. Astrophys.* **103**, 331. ADS.

Kuznetsov, A.A., Chrysaphi, N., Kontar, E.P., Motorina, G.: 2020, Radio Echo in the Turbulent Corona and Simulations of Solar Drift-pair Radio Bursts. *Astrophys. J.* **898**, 94. DOI. ADS.

Lemen, J.R., Title, A.M., Akin, D.J., Boerner, P.F., Chou, C., Drake, J.F., Duncan, D.W., Edwards, C.G., Friedlaender, F.M., Heyman, G.F., Hurlburt, N.E., Katz, N.L., Kushner, G.D., Levay, M., Lindgren, R.W., Mathur, D.P., McFeaters, E.L., Mitchell, S., Rehse, R.A., Schrijver, C.J., Springer, L.A., Stern, R.A., Tarbell, T.D., Wuelser, J.-P., Wolfson, C.J., Yanari, C., Bookbinder, J.A., Cheimets, P.N., Caldwell, D., Deluca, E.E., Gates, R., Golub, L., Park, S., Podgorski, W.A., Bush, R.I., Scherrer, P.H., Gummin, M.A., Smith, P., Auker, G., Jerram, P., Pool, P., Soufli, R., Windt, D.L., Beardsley, S., Clapp, M., Lang, J., Waltham, N.: 2012, The Atmospheric Imaging Assembly (AIA) on the Solar Dynamics Observatory (SDO). *Solar Phys.* **275**, 17. DOI. ADS.

Lin, R.P., Dennis, B.R., Hurford, G.J., Smith, D.M., Zehnder, A., Harvey, P.R., Curtis, D.W., Pankow, D., Turin, P., Bester, M., Csillaghy, A., Lewis, M., Madden, N., van Beek, H.F., Appleby, M., Raudorf, T., McTiernan, J., Ramaty, R., Schmahl, E., Schwartz, R., Krucker, S., Abiad, R., Quinn, T., Berg, P., Hashii, M., Sterling, R., Jackson, R., Pratt, R., Campbell, R.D., Malone, D., Landis, D., Barrington-Leigh, C.P., Slassi-Sennou, S., Cork, C., Clark, D., Amato, D., Orwig, L., Boyle, R., Banks, I.S., Shirey, K., Tolbert, A.K., Zarro, D., Snow, F., Thomsen, K., Henneck, R., McHedlishvili, A., Ming, P., Fivian, M., Jordan, J., Wanner, R., Crubb, J., Preble, J., Matranga, M., Benz, A., Hudson, H., Canfield, R.C., Holman, G.D., Crannell, C., Kosugi, T., Emslie, A.G., Vilmer, N., Brown, J.C., Johns-Krull, C., Aschwanden, M., Metcalf, T., Conway, A.: 2002, The Reuven Ramaty High-Energy Solar Spectroscopic Imager (RHESSI). *Solar Phys.* **210**, 3. DOI. ADS.

Luo, Y., Chen, B., Yu, S., Bastian, T.S., Krucker, S.: 2021, Radio Spectral Imaging of an M8.4 Eruptive Solar Flare: Possible Evidence of a Termination Shock. *Astrophys. J.* **911**, 4. DOI. ADS.

Meegan, C., Lichti, G., Bhat, P.N., Bissaldi, E., Briggs, M.S., Connaughton, V., Diehl, R., Fishman, G., Greiner, J., Hoover, A.S., van der Horst, A.J., von Kienlin, A., Kippen, R.M., Kouveliotou, C., McBreen, S., Paciesas, W.S., Preece, R., Steinle, H., Wallace, M.S., Wilson, R.B., Wilson-Hodge, C.: 2009, The Fermi Gamma-ray Burst Monitor. *Astrophys. J.* **702**, 791. DOI. ADS.

Melnik, V.N., Shevchuk, N.V., Konovalenko, A.A., Rucker, H.O., Dorovskyy, V.V., Poedts, S., Lecacheux, A.: 2014, Solar Decameter Spikes. *Solar Phys.* **289**, 1701. DOI. ADS.

Melrose, D.B.: 2017, Coherent emission mechanisms in astrophysical plasmas. *Reviews of Modern Plasma Physics* **1**, 5. DOI. ADS.

Melrose, D.B., Dulk, G.A.: 1982, Electron-cyclotron masers as the source of certain solar and stellar radio bursts. *Astrophys. J.* **259**, 844. DOI. ADS.

Messmer, P., Benz, A.O.: 2000, The Minimum bandwidth of narrowband spikes in solar flare decimetric radio waves. *Astron. Astrophys.* **354**, 287. ADS.

Motorina, G.G., Fleishman, G.D., Kontar, E.P.: 2020, Spatiotemporal Energy Partitioning in a Nonthermally Dominated Two-loop Solar Flare. *Astrophys. J.* **890**, 75. DOI. ADS.

Ni, S., Chen, Y., Li, C., Zhang, Z., Ning, H., Kong, X., Wang, B., Hosseinpour, M.: 2020, Plasma Emission Induced by Electron Cyclotron Maser Instability in Solar Plasmas with a Large Ratio of Plasma Frequency to Gyrofrequency. *Astrophys. J. Lett.* **891**, L25. DOI. ADS.

Nita, G.M., Fleishman, G.D., Gary, D.E., Marin, W., Boone, K.: 2014, Fitting FFT-derived Spectra: Theory, Tool, and Application to Solar Radio Spike Decomposition. *Astrophys. J.* **789**, 152. DOI. ADS.

Robinson, R.D.: 1983, Scattering of radio waves in the solar corona. *Astronomical Society of Australia, Proceedings (ISSN 0066-9997)* **5**, 208. DOI. ADS.

Scherrer, P.H., Schou, J., Bush, R.I., Kosovichev, A.G., Bogart, R.S., Hoeksema, J.T., Liu, Y., Duvall, T.L., Zhao, J., Title, A.M., Schrijver, C.J., Tarbell, T.D., Tomczyk, S.: 2012, The Helioseismic and Magnetic Imager (HMI) Investigation for the Solar Dynamics Observatory (SDO). *Solar Phys.* **275**, 207. DOI. ADS.

Schou, J., Scherrer, P.H., Bush, R.I., Wachter, R., Couvidat, S., Rabello-Soares, M.C., Bogart, R.S., Hoeksema, J.T., Liu, Y., Duvall, T.L., Akin, D.J., Allard, B.A., Miles, J.W., Rairden, R., Shine, R.A., Tarbell, T.D., Title, A.M., Wolfson, C.J., Elmore, D.F., Norton, A.A., Tomczyk, S.: 2012, Design and Ground Calibration of the Helioseismic and Magnetic Imager

(HMI) Instrument on the Solar Dynamics Observatory (SDO). *Solar Phys.* **275**, 229. DOI. ADS.

Staehli, M., Magun, A.: 1986, The Microwave Spectrum of Solar Millisecond Spikes. *Solar Phys.* **104**, 117. DOI. ADS.

Stepanov, A.V., Kliem, B., Krüger, A., Hildebrand t, J., Garaimov, V.I.: 1999, Second-Harmonic Plasma Radiation of Magnetically Trapped Electrons in Stellar Coronae. *Astrophys. J.* **524**, 961. DOI. ADS.

Tajima, T., Benz, A.O., Thaker, M., Leboeuf, J.N.: 1990, Enhanced Radiation Driven by a DC Electric Field. *Astrophys. J.* **353**, 666. DOI. ADS.

Wentzel, D.G.: 1991, Direct Radiation from a Strong DC Electric Field. *Astrophys. J.* **373**, 285. DOI. ADS.

Willes, A.J., Robinson, P.A.: 1996, Electron-Cyclotron Maser Theory for Noninteger Ratio Emission Frequencies in Solar Microwave Spike Bursts. *Astrophys. J.* **467**, 465. DOI. ADS.

Zhelezniakov, V.V., Zlotnik, E.I.: 1975, Cyclotron Wave Instability in the Corona and Origin of Solar Radio Emission with Fine Structure. I: Bernstein Modes and Plasma Waves in a Hybrid Band. *Solar Phys.* **43**, 431. DOI. ADS.

Zlotnik, E.Y.: 2013, Instability of Electrons Trapped by the Coronal Magnetic Field and Its Evidence in the Fine Structure (Zebra Pattern) of Solar Radio Spectra. *Solar Phys.* **284**, 579. DOI. ADS.